Conference on Modelling Fluid Flow (CMFF'09)
The 14th International Conference on Fluid Flow Technologies
Budapest, Hungary, September 9-12, 2009

VALIDATION OF THE 2D NUMERICAL INVESTIGATION METHODOLOGY OF THE TURBULENT FLOW INTO AN INDUCER WITH THE 3D COMPUTATION

Adrian STUPARU[1], Sebastian MUNTEAN[2], Liviu ANTON[3]

[1] Corresponding Author. Department of Hydraulic Machinery, University Politehnica of Timisoara, Mechanical Engineering Faculty. Blv. Mihai Viteazu, RO-300222, Timisoara, Romania. Tel.: +40 0256 403698, Fax: +42 0256 403692, E-mail: astuparu@mh.mec.upt.ro
[2] Centre of Advanced Research in Engineering Sciences Romanian Academy - Timisoara Branch. E-mail: seby@mh.mec.upt.ro
[3] Department of Hydraulic Machinery, University Politehnica of Timisoara, Mechanical Engineering Faculty. E-mail: liviu.anton@mec.upt.ro

ABSTRACT (STYLE: ABSTRACT TITLE)

Keywords: inducer, 2D and 3D flow simulation, pressure distribution

NOMENCLATURE

Q	[m^3/s]	flow rate
n	[rpm]	rotational speed
s	[mm]	thickness
$\underline{\beta_s}$	[^{o}]	stager angle
$\underline{\beta_0}$	[^{o}]	inflow angle
t/l	[-]	space/chord ratio
w	[m/s]	relative velocity
v	[m/s]	absolute velocity
S	[m^2]	aria of the section
ρ	[kg/m^3]	density
t	[s]	time
g	[m/s^2]	gravitational acceleration
w	[m/s]	relative velocity
p	[Pa]	static pressure
c_p	[-]	static pressure coefficient
μ	[kg/m-s]	dynamic viscosity
ω	[rad/s]	angular speed

Subscripts and Superscripts

IN	at the inlet of the test section
PS, SS	pressure side, suction side
x, y,	axial (along the wind tunnel axis), transversal (coordinate)

1. INTRODUCTION

The inducer is an axial impeller which is mounted on the same shaft with the impeller of a pump. Because it increases the pressure over the vaporising pressure, the inducer reduces the cavitation by producing a supplementary specific energy on the inlet of the impeller of the pump. The inducer is used for the pumps with severe suction condition and it has a "sacrificial role". It will be replaced after a certain operating time and that is why the technology for its execution has to be simple and economical. The use of straight hydrofoil cascade for the construction of the blades of the inducer satisfies these requirements.

The aim of this paper is to compare the results of the flow simulation obtained with 2D, which is used in the designing process, and 3D numerical investigation into an inducer.

In order to validate the 2D and 3D numerical investigations of the flow, the distribution of the pressure coefficient for 3 sections of the blade (near the hub, middle and near the shroud) is compared with the experimental measurements of the pressure coefficient obtained from the investigations performed in a test rig upon the inducer.

2. EXPERIMENTAL TEST RIG

The inducer presented in Figure 1, has the hydrofoil cascade formed by straight hydrofoil with a rounded leading and trailing edge, has two blades and was numerical and experimental investigated

Figure 1. The investigated inducer

The test rig for the experimental investigation of the flow in an inducer is presented in Figure 2.

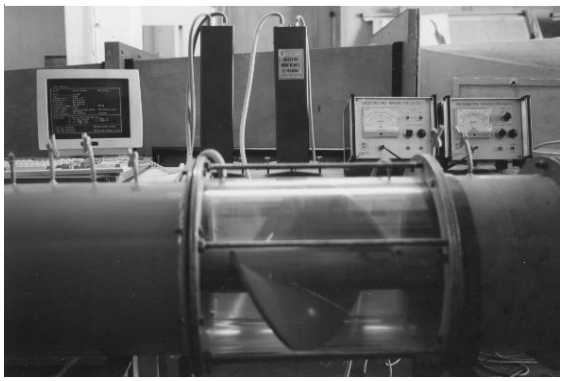

Figure 2. Test rig for pressure measurement on the blade of an inducer

This is a wind tunnel in open circuit with the radius of the measuring section of 300 mm. The inducer model has drained blades and allowed, through two scan valves sealed with magnetic fluid, the measurement and the calculation of the pressure distribution along the blades.

2. COMPUTATIONAL DOMAINS AND BOUNDARY CONDITIONS

2.1. Computational domain and boundary conditions for 2D flow simulation

The 2D flow simulation is performed because this is the basis for the classical designing method of an inducer.

The geometrical characteristic of the hydrofoil corresponds to the middle radius of the blade and the investigated operating conditions are given in table 1:

Table 1. Geometrical characteristic and operating conditions of the investigated hydrofoil of the inducer

Q [m^3/s]	n [rpm]	s [mm]	β_s [°]	β_0 [°]	t/l [-]
0.336	1450	9	36.5	17.9	0.804

The computational domain, Figure 3, was generated using the pre-processor GAMBIT from FLUENT, based on actual geometry.

The structured mesh for the 2D computational domain is generated with 60,000 cells. A boundary layer was attached to the hydrofoil in order to be able to compute correctly the flow into the boundary layer.

The periodic boundaries of the domain are located at a distance, regarding the chord, equal with the space of the cascade, while the inlet is positioned at a distance equal with half of the space of the cascade and the outlet at a distance equal with four times the space of the cascade.

Figure 3. 2D computational domain of the inducer

We imposed on the inlet section of the 2D computational domain the two components of the relative velocity, Eq. (1) and Eq. (2), corresponding to the prescribed flow rate and flow angle, together with the turbulence parameters, a turbulent intensity of 1% and a hydraulic diameter of 0.3 m.

$$w_x = \frac{Q}{S_{IN}} = 4.757 \text{ m/s} \quad (1)$$

$$w_y = \frac{w_x}{tg\beta_0} = 14.728 \text{ m/s} \quad (2)$$

On the outlet section of the computational domain a radial equilibrium condition is chosen.

On the periodic surfaces of the domains the periodicity of the velocity, pressure and turbulence parameters were imposed.

The remaining boundary conditions for the domain correspond to zero relative velocity.

2.2. Computational domain and boundary conditions for 3D flow simulation

The 3D numerical flow analyze is performed because of the limitations of the 2D method in the investigation of the real flow inside an inducer.

The first generated mesh for the 3D computational domain, Figure 4, is structured and has 460,000 cells. The second mesh is obtained from refining the first mesh in the region of the leading edge of the blade and pressure side and suction side of the blade, so that the value of the Y+ to be smaller.

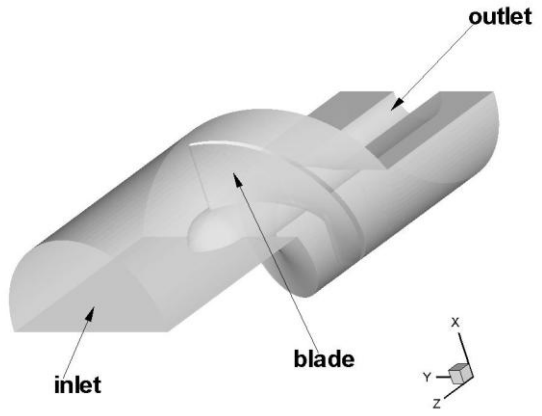

Figure 4. 3D computational domain of the inducer

For the inlet section of the 3D computational domain the velocity, corresponding to the prescribed discharge, Eq. (3) together with the turbulence parameter, a turbulent intensity of 1% and a hydraulic diameter of 0.3 m, is imposed.

$$v = \frac{Q}{S_{IN}} = 4.757 \text{ m/s} \tag{3}$$

On the outlet section of the computational domain a radial equilibrium condition is chosen.

On the periodic surfaces of the domains the periodicity of the velocity, pressure and turbulence parameters were imposed.

The remaining boundary conditions for the domain correspond to zero relative velocity.

3. NUMERICAL METHOD

For the flow analysis presented in this paper we consider a 2D turbulent flow model. A steady relative flow is computed in the computational domain.

$$\nabla \cdot \vec{v} = 0 \tag{4}$$

$$\frac{d\ \rho\vec{v}}{dt} = \rho g - \nabla p + \mu \Delta \vec{v} \tag{5}$$

The numerical solution of flow equations (1) and (2) is obtained with the expert code FLUENT 6.3.26, using a Reynolds-averaged Navier-Stokes (RANS) solver.

Based on previous research work, the turbulent viscosity is computed using the Reynolds Stress Model (RSM).

The Reynolds stress model (RSM) is the most elaborate turbulence model that **FLUENT** provides. Abandoning the isotropic eddy-viscosity hypothesis, the RSM closes the Reynolds-averaged Navier-Stokes equations by solving transport equations for the Reynolds stresses, together with an equation for the dissipation rate. This means that five additional transport equations are required in 2D flows and seven additional transport equations must be solved in 3D.
Since the RSM accounts for the effects of streamline curvature, swirl, rotation, and in a more rigorous manner than one-equation and two-equation models, it has greater potential to give accurate predictions for complex flows. However, the fidelity of RSM predictions is still limited by the closure assumptions employed to model various terms in the exact transport equations for the Reynolds stresses. The modeling of the pressure-strain and dissipation-rate terms is particularly challenging, and often considered to be responsible for compromising the accuracy of RSM predictions.

For the 3D turbulent flow simulation we solve a relative flow, in a rotating frame of reference with angular speed

$$\vec{\omega} = \omega \vec{k} \tag{6}$$

$\vec{k}$ being the unit vector of the inducer axis direction.

By introducing the relative velocity

$$\vec{w} = \vec{v} - \vec{\omega} \times \vec{r} \tag{7}$$

with $\vec{r}$ the position vector, the left hand side of (6) becomes

$$\frac{\partial}{\partial t}\ \rho\vec{w}\ + \nabla \cdot\ \rho\vec{w}\vec{w}\ + 2\rho\vec{\omega} \times \vec{w} + \\ + \rho\vec{\omega} \times\ \vec{\omega} \times \vec{r}\ + \rho \frac{\partial \vec{\omega}}{\partial t} \times r \tag{8}$$

An important assumption used in the present computation is that the relative flow is steady. This simplifies (8) by removing the first and last terms, and also allows the computation of flow on a single inter-blade channel.

The same turbulence model, RSM, was used for the 3D numerical simulation of the turbulent flow.

4. NUMERICAL RESULTS

The pressure coefficient is defined by the following equation:

$$c_p = \frac{p - p_{IN}}{\frac{\rho}{2} w_{IN}^2} \tag{9}$$

For the validation of the numerical results, a comparison between the pressure coefficient

computed in the 2D numerical investigation against experimental data is plotted in Figure 5.

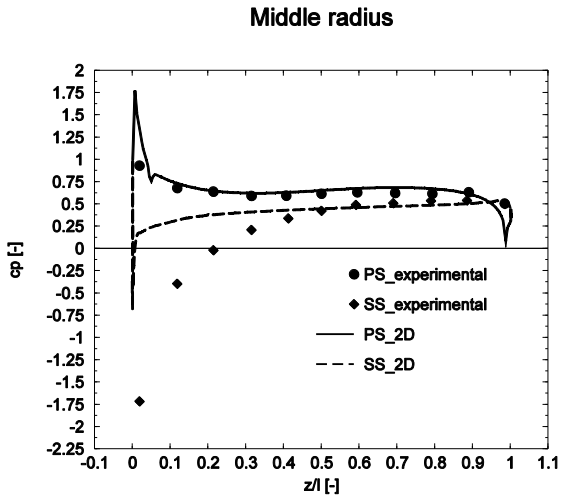

Figure 5. Pressure coefficient distribution along the blade of the inducer, at the middle radius, for 2D domain

From the comparison of the numerical and experimental, [1], pressure coefficient distribution along the blade, Figure 3, it results a good agreement for the pressure side of the blade. It can be observed that on the suction side of the blade appears a difference between the numerical data and the experimental one, for the first part of the blade. This happens because in that region of the blade appears a recirculation of the fluid. The cause for the fluid recirculation is the point of incidence of the fluid. This point is not positioned on the leading edge of the blade, as it should be, but it is shifted towards the pressure side of the hydrofoil.

In Figure 6 the streamlines for the hydrofoil cascade is presented.

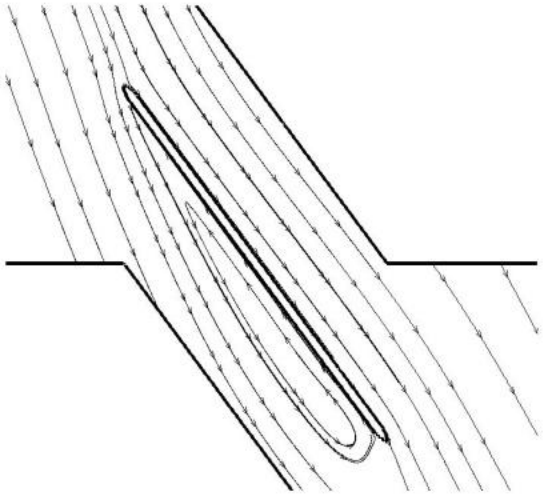

Figure 6. Distribution of the streamlines, at the middle radius, for 2D domain

It can be observed from Figure 6 the recirculation zone on the suction side, which leads to the partial blockage of the flow channel.

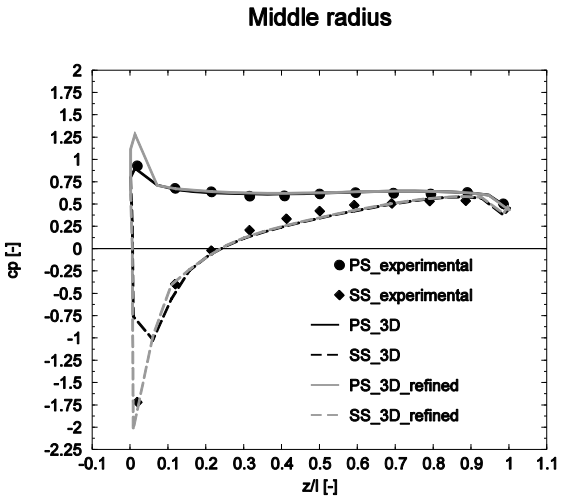

Figure 7. Pressure coefficient distribution along the inducer blade, at radius r = 0.111 m, for the 3D domain

From Figure 7 it can be observed a very good agreement between the data obtained from numerical simulations for the two types of mesh and the experimental data. The distribution of the pressure coefficient obtained from 3D numerical simulation for the refined mesh catches the leap of the pressure coefficient near the leading edge.

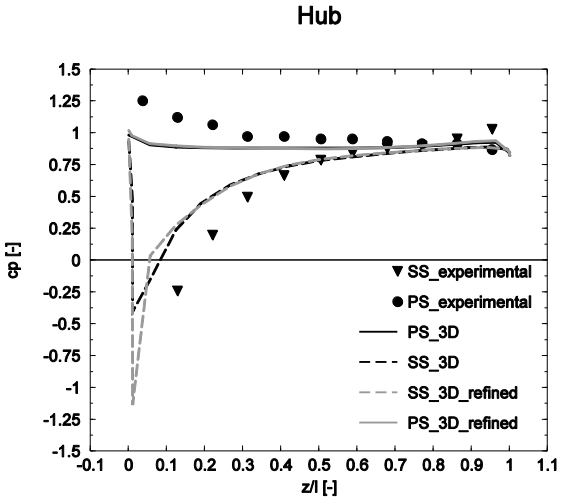

Figure 8. Pressure coefficient distribution along the inducer blade, at radius r = 0.05 m, for the 3D domain

The pressure coefficient distribution near the hub, Figure 8, obtained from 3D numerical simulation for the two types of mesh is not very similar with the experimental one, for the suction side and pressure side of the blade.

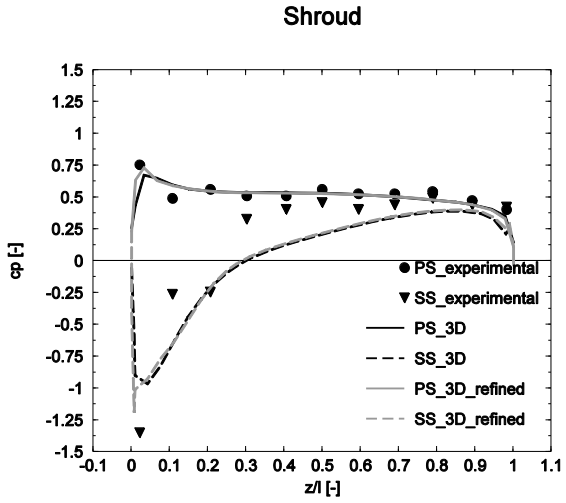

Figure 9. Pressure coefficient distribution along the inducer blade, at radius r = 0.145 m, for the 3D domain

The distribution of the pressure coefficient near the shroud, Figure 9, on the pressure side of the blade is similar with the experimental one, for both types of mesh. For the suction side of the blade the distribution of the pressure coefficient obtained from 3D numerical simulation of the flow for the both types of mesh is not similar with the measured pressure coefficient.

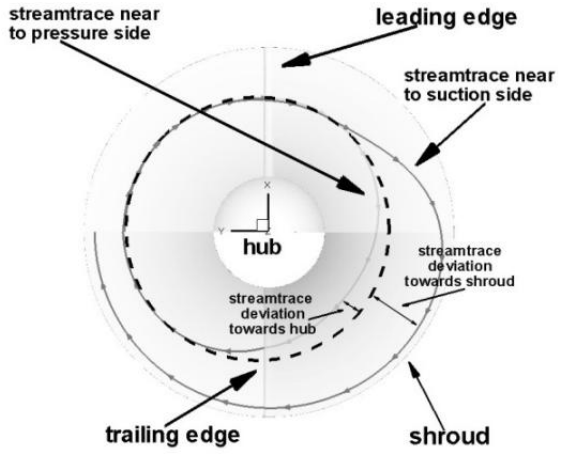

Figure 10. 3D effects on the loading of the inducer blade for stream trace positioned at r = 0.111 m

The 3D effects due to the loading of the inducer blade lead to the deviation of the stream trace towards the hub on the pressure side and towards the shroud on the suction side, Figure 10. The flow on the pressure side towards the blade exit is positioned at the same radius as on the inlet of the blade. Moreover, the stream trace near to the pressure side moves near to the blade, while the stream trace on the suction side is pushed away from the blade, Figure 11.

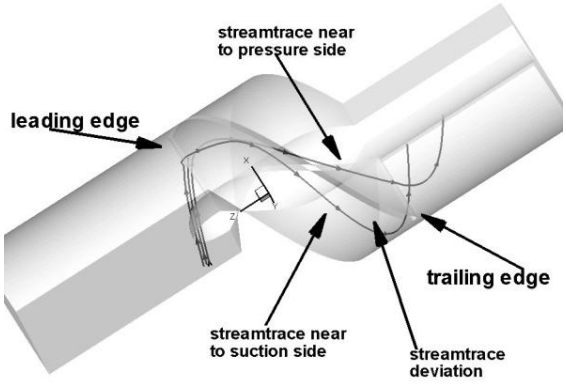

Figure 11. 3D deviation of the stream trace on the suction side

5. CONCLUSIONS

REFERENCES

[1] Anton, L. E. 1994, "Determination of pressure distribution on the blades of an inducer", *Proceedings of XVII IAHR Symposium*, pp. 321-328, China, September, Beijing.

[2] Susan-Resiga, R.; 1999, "Periodic boundary conditions implementation for the Finite Element Analysis of Cascade Flows", *Scientific bulletin of Politehnica University Timisoara*, Vol. 44(58), pp. 151-160.

[3] Fluent Inc., 2005, *FLUENT 6.3 User's Guide*, Fluent Incorporated, Lebanon

[4] Fluent Inc., 2005, *GAMBIT 2.2.30 User's Guide*, Fluent Incorporated, Lebanon